Supporting Information

Medium-Entropy State Quinary Keplerate Clusters as Remarkable Electrocatalyst for Small Molecule Electrooxidation

Mengyang Cao[a+], Hongfang Ye[a+], Yingying Liu[a], Jianwen Wang[a], Yin Zhou[a], Xianwen Wang[a], Shining Wu[a], Feng Xu[a*], Yingpeng Wu[a*]

[a] State Key Laboratory of Chem/Bio-Sensing and Chemometrics, Advanced Catalytic Engineering Research Center of the Ministry of Education, College of Chemistry and Chemical Engineering, Hunan University, Changsha, 410082, P. R. China.

[+] Mengyang Cao and Hongfang Ye contributed equally to this paper

* Email: feng_xu@hnu.edu.cn , wuyingpeng@hnu.edu.cn

Table of Contents

Figure S1. The photograph of solution products. Solution product images of M20-20 (left), M20-9 (middle) and M20-7 (right).

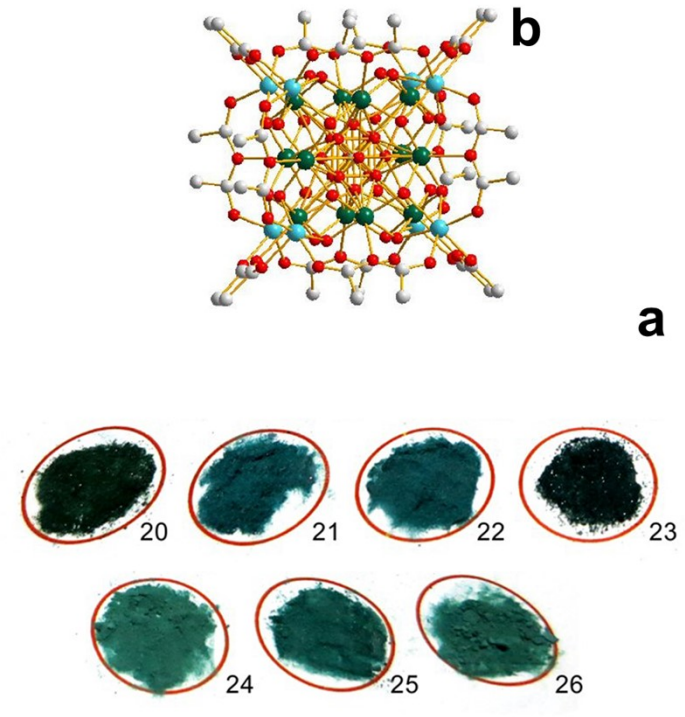

Figure S2. Image of single crystal samples of M20-20 ~M20-26 and a ball-and-stick model of {M_{20}}. (a) Image of 7 single crystal samples of M20-20 ~M20-26. (b) A ball-and-stick representation of the discrete clusters {M_{20}}. The structure contains 20 disordered Cu^{2+}, Ni^{2+}, Co^{2+}, Mn^{2+} and Zn^{2+} ions. H atoms, lattice acetates and water molecules have been omitted for clarity. Color scheme: Ni/Co/Mn/Cu/ Zn, blue and dark green; O, red; C, gray.

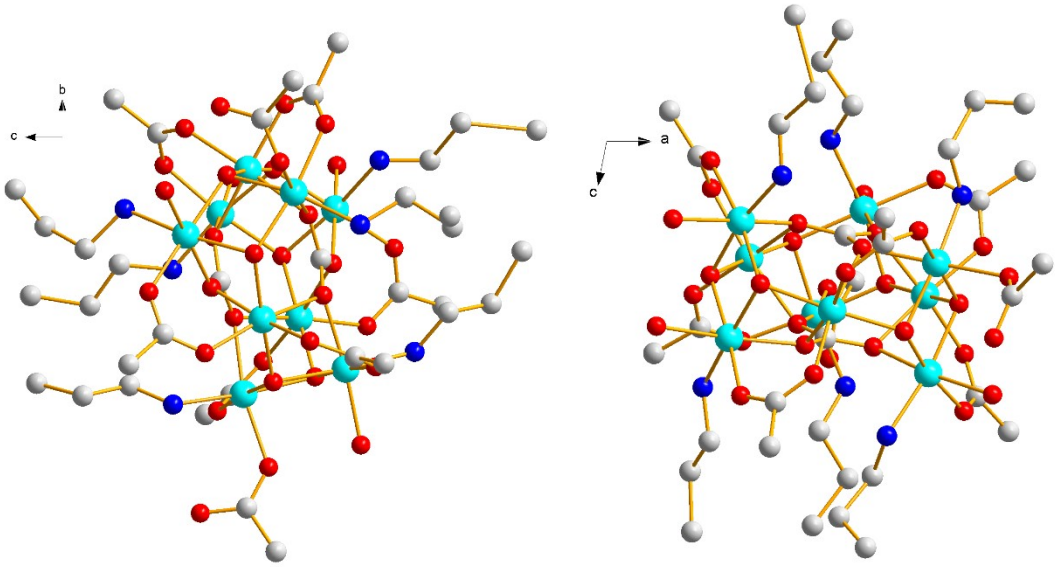

Figure S3. Structure of the {Ni_9} cluster. Structure of the {Ni_9} cluster obtained from the reaction using only $Ni(OAc)_2$ as the starting material. Color scheme: Cu, light blue; N, dark blue; O, red; C, gray.

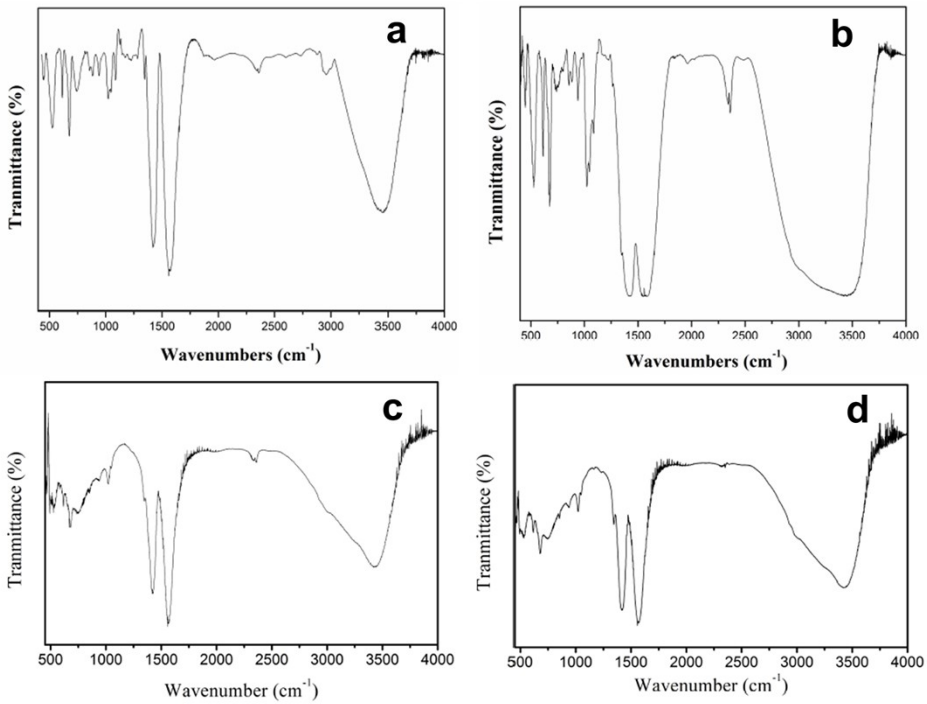

Figure S4. IR spectra of M20-7, M20-9, M20-17, M20-20. IR spectra of (a) M20-7 (Cu-Ni), (b) M20-9 (Cu-Co), (c) M20-17 (Cu-Ni-Co) and (d) M20-20 (Cu-Ni-Co-Zn-Mn), shows their resemblance.

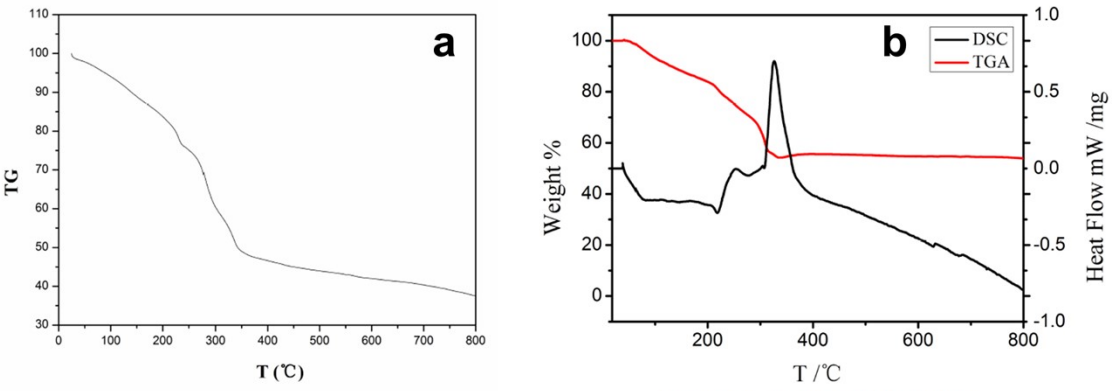

Figure S10. TGA/DSC of **M20-17** in N_2 flow.

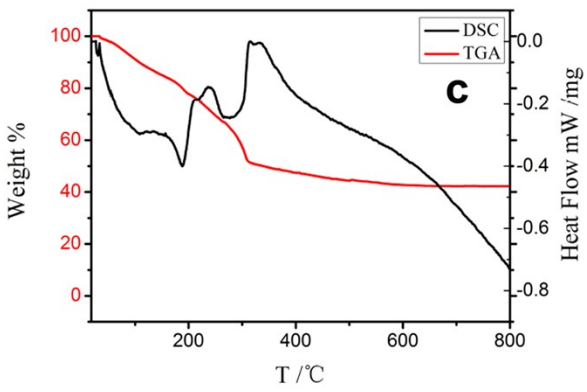

91

92

93 **Figure S5. TGA of M20-7, M20-17, M20-20.** (a)TGA of M20-7 in N_2 flow. (b)TGA/DSC of M20-17

94 in N_2 flow. (c) TGA/DSC of M20-20 in N_2 flow.

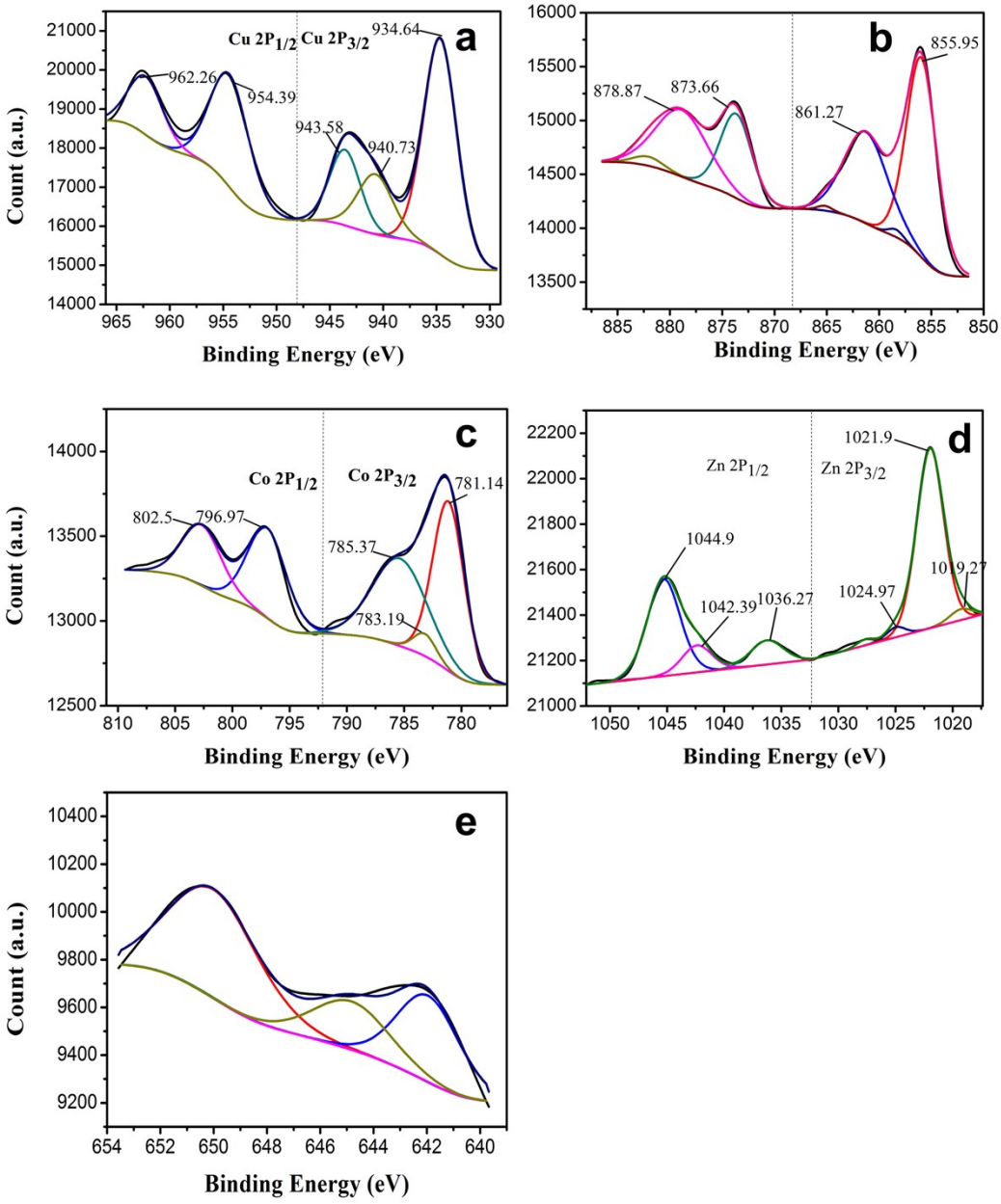

Figure S6. The XPS spectra for as-synthesized M20-20. (a) 934.64 eV is ascribed to Cu $2P_{3/2}$ and 954.39 eV is relative to Cu $2P_{1/2}$ of Cu^{2+}. (b) Ni $2P_{3/2}$ and Ni $2P_{1/2}$ signals of Ni^{2+} are at 856 and 873 eV, respectively. (c) Co $2P_{3/2}$ and Co $2P_{1/2}$ signals of Co^{2+} are at 781.3 and 797.3 eV. (d) The peaks at 1021.9 and 1044.27 eV belong to the Zn $2P_{3/2}$ and Zn $2P_{1/2}$ signals of Zn^{2+}. (e) The peaks at 641.95 and 649.09 eV are ascribed to the Mn $2P_{3/2}$ and Mn $2P_{1/2}$ signals of Mn^{2+}, respectively.

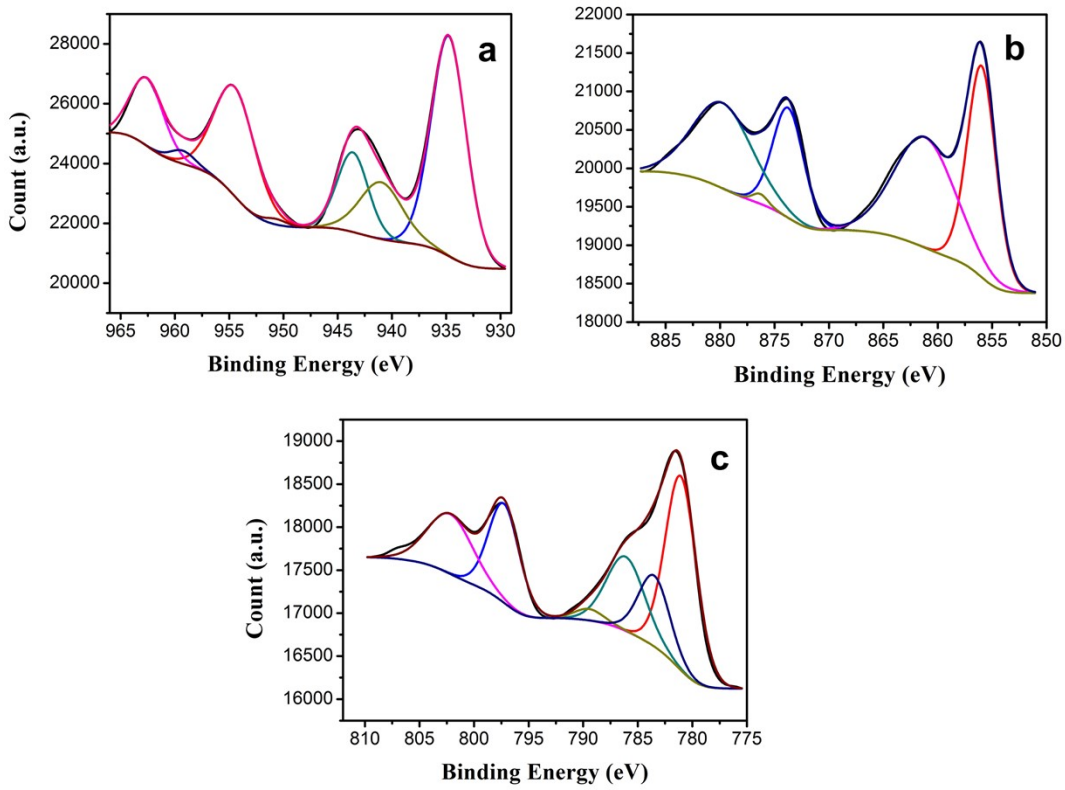

Figure S7. The XPS spectra for as-synthesized M20-17. (a) The peaks at 935 and 954.8 eV are ascribed to the Cu $2P_{3/2}$ and Cu $2P_{1/2}$ of Cu^{2+}, respectively. The other peaks located at higher binding energies (940-945 eV and 954-965 eV) can be attributed to satellite peaks characteristic of Cu^{2+}. (b) The peaks at 856 and 873 eV are ascribed to the Ni $2P_{3/2}$ and Ni $2P_{1/2}$ signals of Ni^{2+} respectively. (c) The peaks at 781.3 and 797.3 eV are ascribed to the Co $2P_{3/2}$ and Co $2P_{1/2}$ signals of Co^{2+}, respectively.

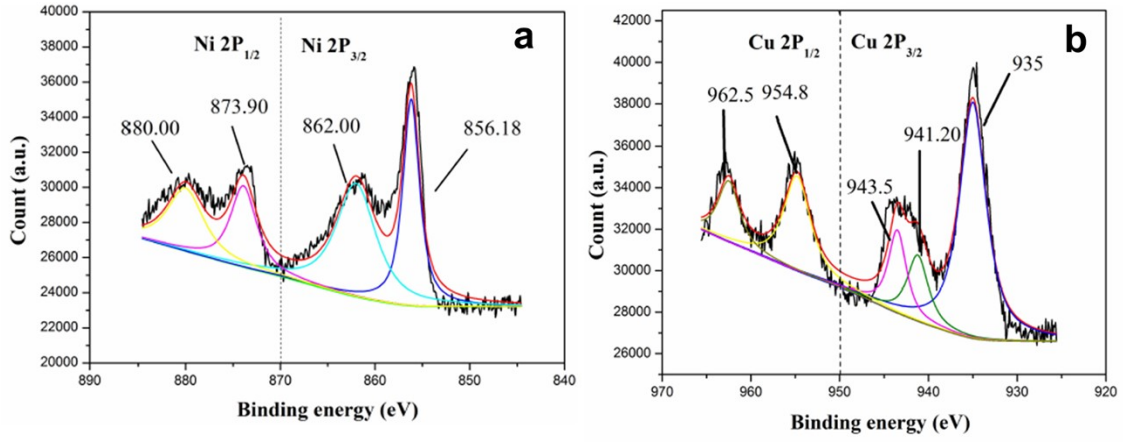

Figure S8. The XPS spectra for as-synthesized M20-7. (a) The peaks at 935 and 954.8 eV are ascribed to the Cu $2P_{3/2}$ and Cu $2P_{1/2}$ of Cu^{2+}, respectively. The other peaks located at higher binding energies (940-945 eV and 954-965 eV) can be attributed to satellite peaks characteristic of Cu^{2+}. (b) The peaks at 856 and 873 eV are ascribed to the Ni $2P_{3/2}$ and Ni $2P_{1/2}$ signals of Ni^{2+}, respectively.

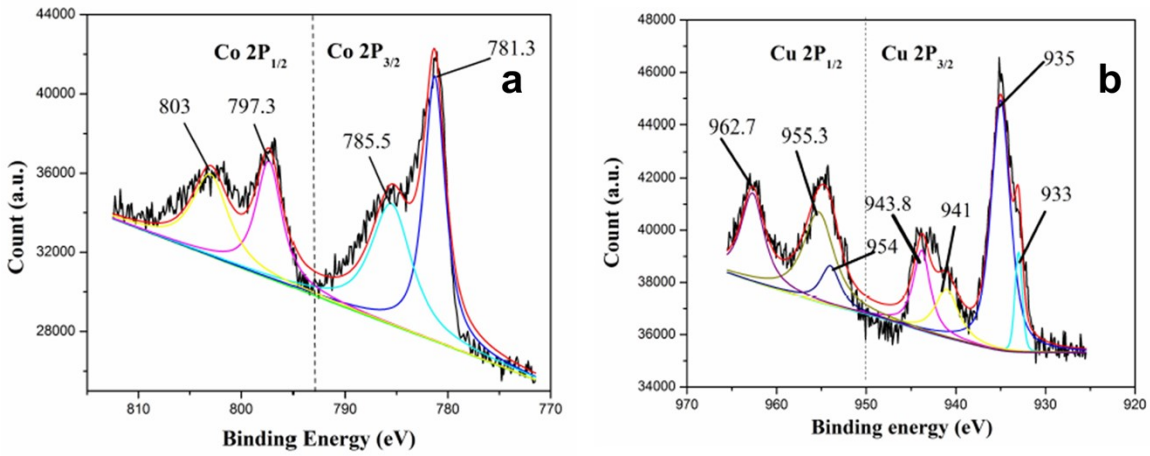

Figure S9. The XPS spectra for as-synthesized M20-9. (a) the peaks at 935 and 955.3 eV are ascribed to the Cu $2P_{3/2}$ and Cu $2P_{1/2}$ of Cu^{2+}, respectively. The other peaks located at higher binding energies (940-945 eV and 954-965 eV) can be attributed to satellite peaks characteristic of Cu^{2+}. (b) The peaks at 781.3 and 797.3 eV are ascribed to the Co $2P_{3/2}$ and Co $2P_{1/2}$ signals of Co^{2+}, respectively.

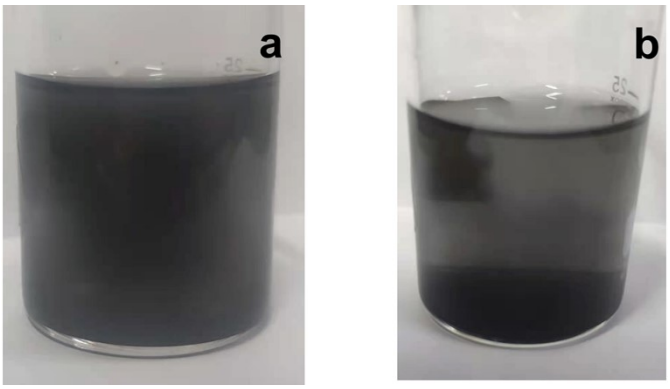

Figure S10. Photograph of NCNT mixed with M20-20. (a) NCNT dispersed in ethanol (b) Mixing solution after addition of M20-20, the precipitate proving the NCNT and M20-20 combined by electrostatic force.

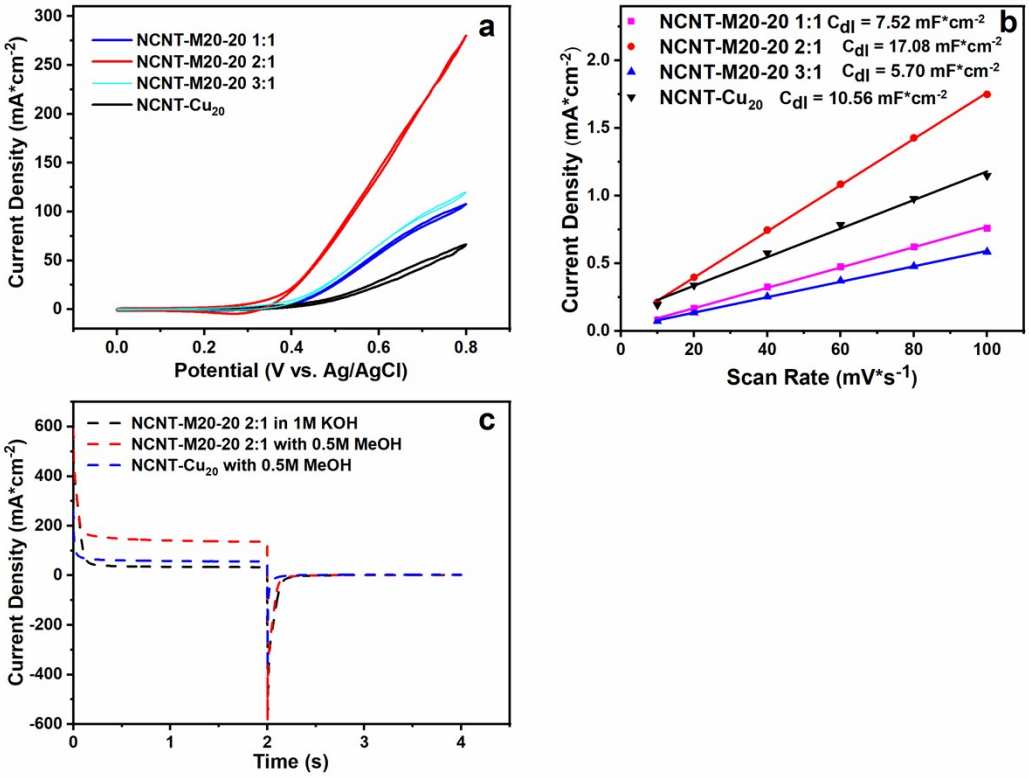

136

137 **Figure S11. Electrooxidation methanol characterization of NCNT-M20-20.** (a) CV comparison
138 of all samples in 1 M KOH with 0.5 M methanol. (b) Electric double-layer capacitance comparison
139 of all samples. (c) Double-step chronoamperometry analysis of NCNT-Cu_{20} and NCNT-M20-20 2:1
140 in 1M KOH with and without 0.5 M methanol.

141

142

143

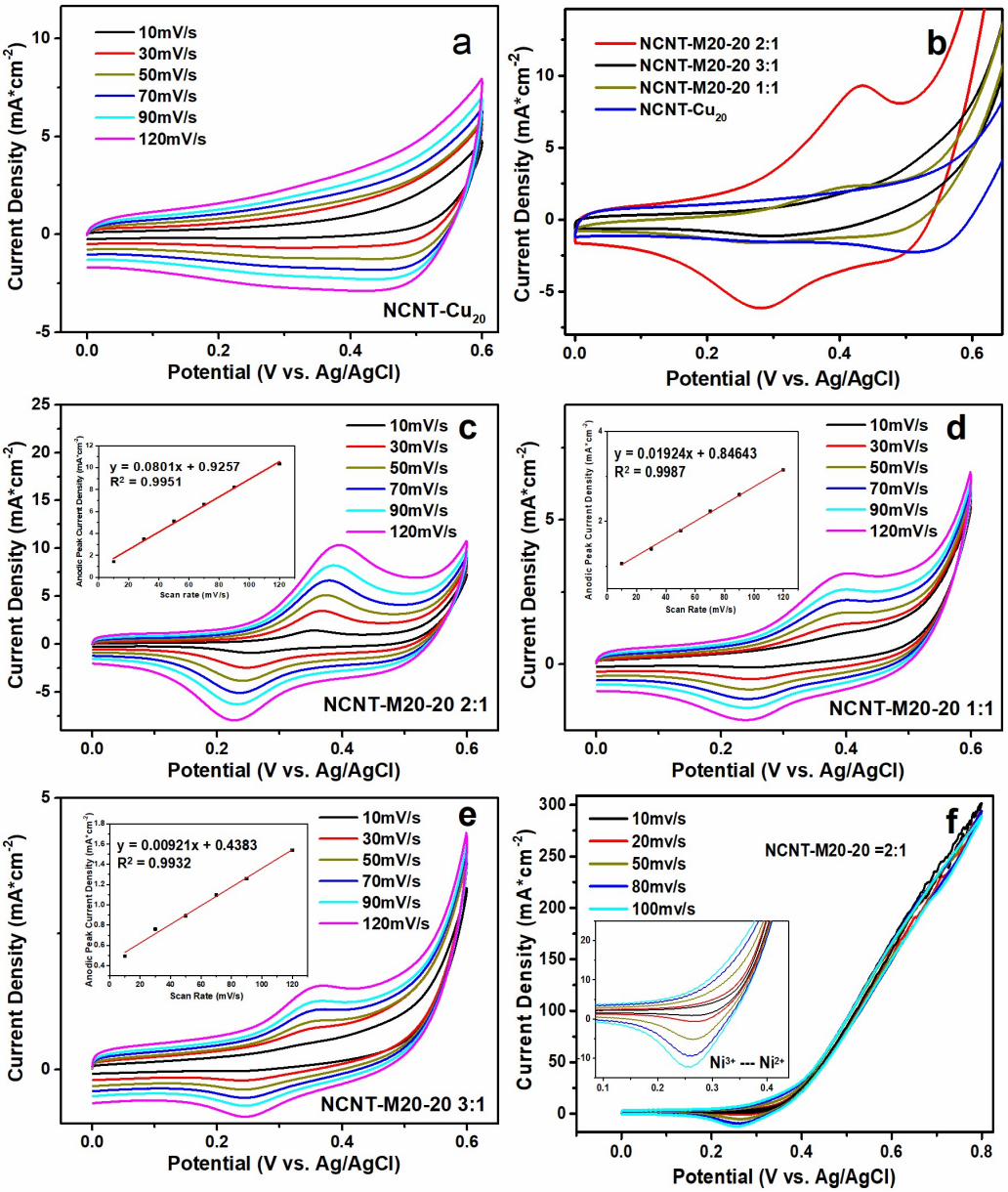

144

145 **Figure S12. Electrochemical behavior analysis of NCNT-M20-20 using CVs with different**
146 **scan rates.** (a) CVs of NCNT-Cu_{20} in 1 M KOH at different scan rates. (b) All samples' CVs in 1 M
147 KOH. (c) CVs of NCNT-M20-20 2:1 in 1 M KOH at different scan rates, the inset graph is the
148 linearity of anodic peak current density vs. scan rate. (d) CVs of NCNT-M20-20 1:1 in 1 M KOH at
149 different scan rates, the inset graph is the linearity of anodic peak current density vs. scan rate. (e)
150 CVs of NCNT-M20-20 3:1 in 1 M KOH at different scan rates, the inset graph is the linearity of

anodic peak current density vs. scan rate. (f) CV curves of NCNT-M20-20 2:1 electrode in 1.0 M KOH + 0.5 M methanol electrolyte at different scan rate, the inset image is partial enlargement of the curve.

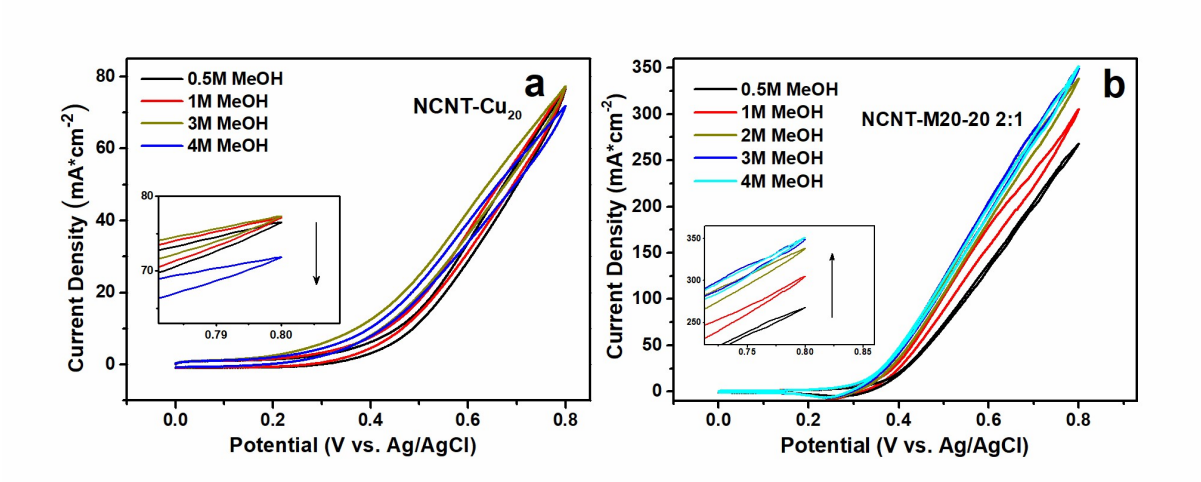

Figure S13. High methanol concentration tolerance test. (a) CV curves of NCNT-Cu_{20} and (b) CVs of NCNT-M20-20 2:1 in 1M KOH with different methanol concentration with magnified view around 0.8V.

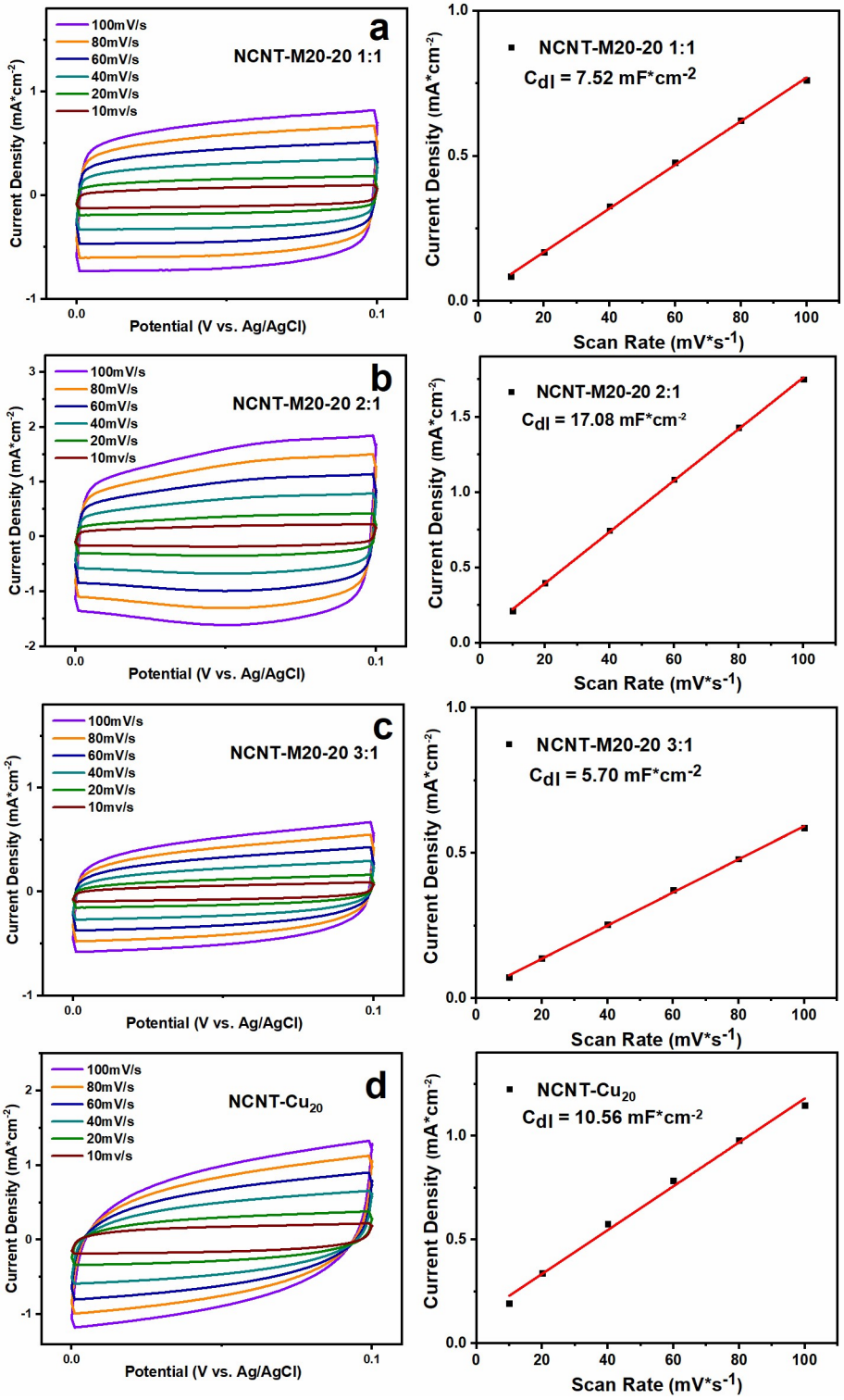

162

163 **Figure S14. Electrochemical active surface area test.** CVs of NCNT-M20-20 1:1(a), 2:1(b),
164 3:1(c), and NCNT-Cu_{20} (d) tested in 1M KOH at increasingly higher sweep rates: 10, 20, 40, 60,

80, 100 mV s^{-1}. The right side is the linear fitting of the anodic current densities to the scan rates of each sample.

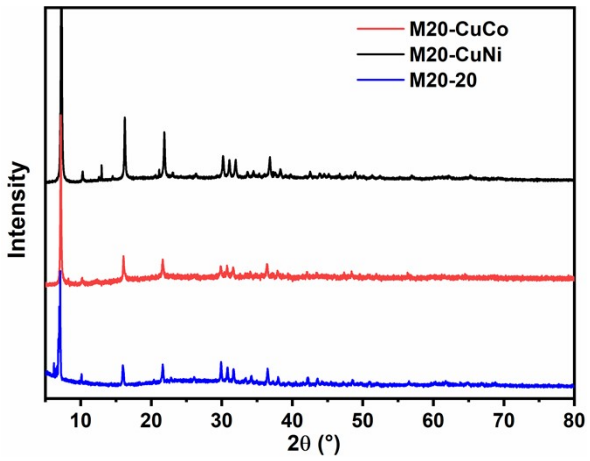

Figure S15. XRD results of M20-CuNi, M20-CuCo and M20-20.

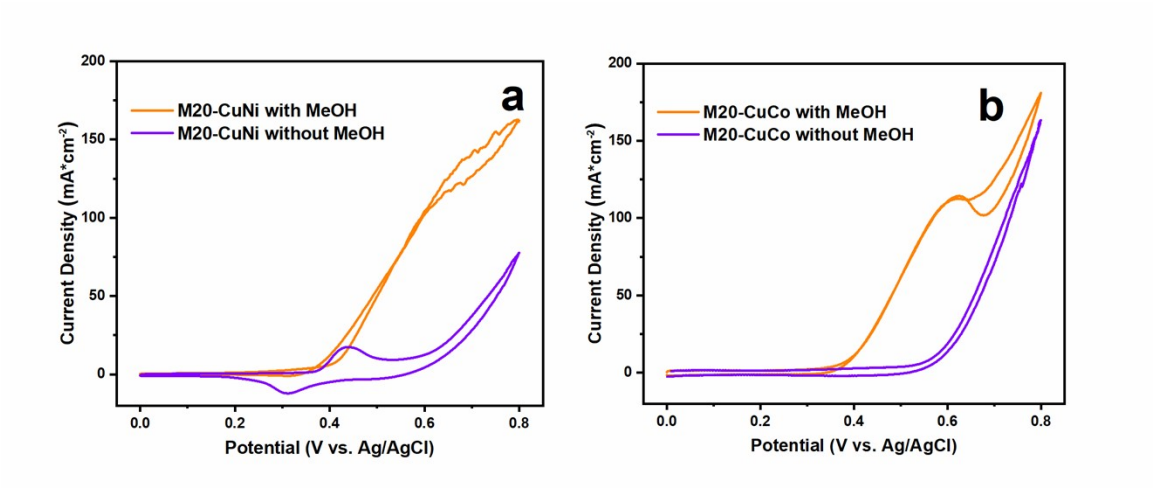

Figure S16. (a) CV comparison of M20-CuNi with and without 0.5M MeOH. **(b)** CV comparison of M20-CuCo with and without 0.5M MeOH.

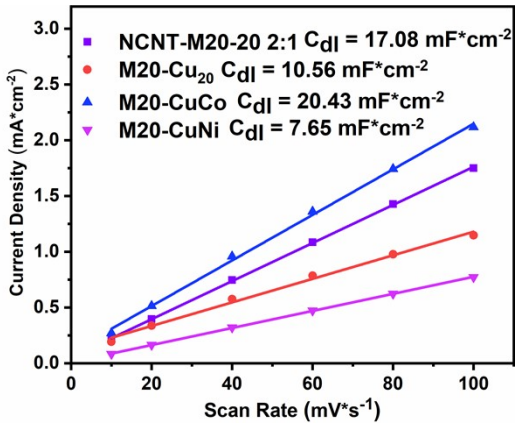

Figure S17. Double layer capacitance comparison of NCNT-M20-20 2:1, M20-Cu_{20}, M20-CuCo, M20-CuNi.

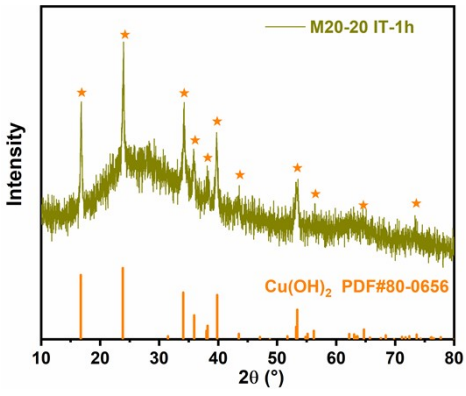

Figure S18. The XRD result of M20-20 after chronoamperometry at 0.7V.

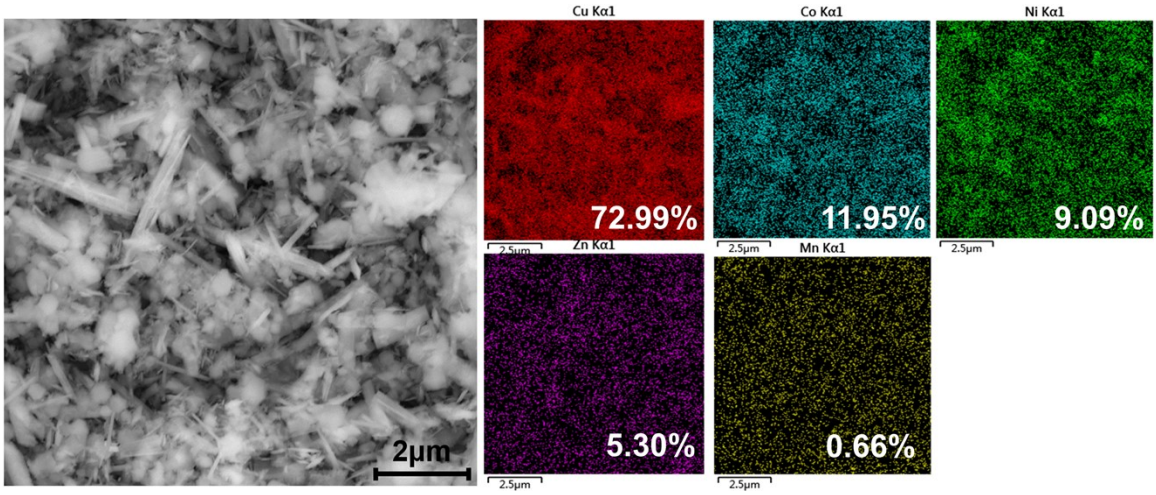

Figure S19. SEM and EDS results of M20-20 after 0.7V, chronoamperometry, metal element proportion marked left bottom at each element distribution.

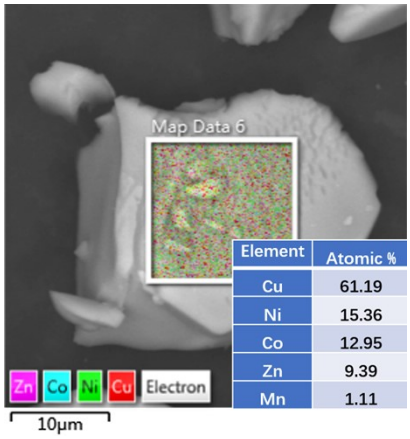

Figure S20. SEM and EDS result of pristine M20-20 bulk with element proportion at

bottom right.

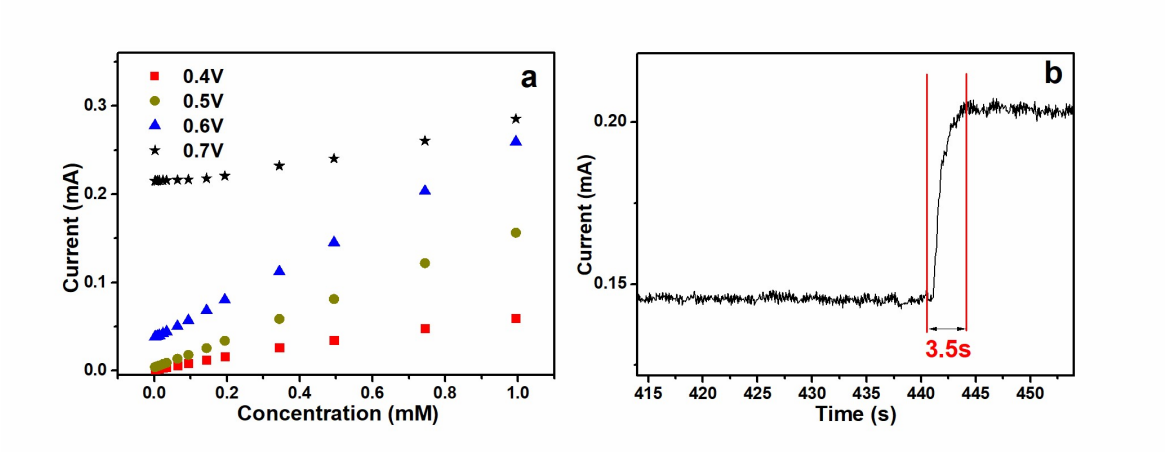

Figure S21. Response time test and working potential optimization for glucose detection. (a) The current–concentration response of NCNT-M20-20 2:1 under different potentials. (b) Amperometric response time for reaching a steady state after glucose injection.

Table S1. Metal composition of the obtained single-crystalline keplerates in {M_{20}} library.

Code	Metal Composition	Ratio[a]	Amines
M20-7	$Cu_{10.38}Ni_{9.62}$	1:1.5	trimethylamine
M20-9	$Cu_{10.77}Co_{9.23}$	1:1	trimethylamine
M20-10	$Cu_{9.80}Co_{10.20}$	1:1.5	trimethylamine
M20-17	$Cu_{10.19}Ni_{4.91}Co_{4.90}$	3:2:3	*iso*-propylamine
M20-19	$Cu_{10.57}Ni_{5.63}Co_{3.13}Zn_{0.67}$	1:1:1:1	trimethylamine

M20-20	$Cu_{12.87}Ni_{2.93}Co_{2.88}Zn_{1.12}Mn_{0.18}$	6:1:1:1:1	*iso*-propylamine
M20-21	$Cu_{9.98}Ni_{5.16}Co_{4.35}Zn_{0.41}Mn_{0.10}$	4:2:2:1:1	*iso*-propylamine
M20-22	$Cu_{9.06}Ni_{4.93}Co_{5.63}Zn_{0.23}Mn_{0.15}$	3:2:3:1:1	*iso*-propylamine
M20-23	$Cu_{9.37}Ni_{6.01}Co_{4.10}Zn_{0.39}Mn_{0.13}$	2:2:2:2:2	*iso*-propylamine
M20-24	$Cu_{11.55}Ni_{3.91}Co_{3.39}Zn_{0.74}Mn_{0.44}$	6:1:1:1:1	trimethylamine
M20-25	$Cu_{10.16}Ni_{5.12}Co_{3.98}Zn_{0.26}Mn_{0.48}$	4:2:2:1:1	trimethylamine
M20-26	$Cu_{9.68}Ni_{4.45}Co_{5.19}Zn_{0.20}Mn_{0.48}$	3:2:3:1:1	trimethylamine

213 [a] Ratio of each metal acetate (mmol) in a 20 mL reaction mixture.

Table S2. Synthetic results of $\{M_{20}\}$ keplerates with different starting metal salts combinations and amines

Metal Combination		Result Products with Different Amine and Precursor Ratio							
	Cu	$\{Cu_{20}\}$							
	Cu-Zn	**3.1:3.1**							
		$\{Cu_{12}Zn_8\}$							
	Cu-Ni	**2:1**		**1:1**		**1:1.5**		**1:2**	
		$Cu_{12.59}Ni_{7.41}$	$Cu_{12.37}Ni_{7.64}$	$Cu_{10.23}Ni_{9.77}$	$Cu_{10.49}Ni_{9.51}$	$Cu_{8.70}Ni_{11.30}$	$Cu_{10.38}Ni_{9.62}$	$Cu_{9.01}Ni_{10.99}$	$Cu_{9.99}Ni_{10.01}$
	Cu-Co	**2:1**		**1:1**		**1:1.5**		**1:2**	
		×	×	×	$Cu_{10.77}Co_{10.23}$	×	$Cu_{9.8}Co_{10.2}$	×	$Cu_{9.41}Co_{10.59}$
	Cu-Ni-Zn	**5:2:2**		**4:2:2**		**3:3:2**		**3:3:3**	
		×	×	×	×	×	$Cu_{11.29}Ni_{8.02}Zn_{0.69}$	×	$Cu_{10.13}Ni_{8.77}Zn_{1.10}$
	Cu-Co-Zn	**5:2:2**		**4:2:2**		**3:3:2**		**3:3:3**	
		×	×	×	×	×	$Cu_{10.49}Co_{8.76}Zn_{0.75}$	×	$Cu_{10.67}Co_{8.14}Zn_{1.19}$
	Cu-Ni-Co	**5:2:2**		**4:2:2**		**3:3:2**		**3:3:3**	
		×	×	$Cu_{11.21}Ni_{5.31}Co_{3.48}$	-	$Cu_{10.20}Ni_{4.91}Co_{4.90}$	-	$Cu_{9.89}Ni_{6.25}Co_{3.86}$	-
	Cu-Ni-Co-Zn	**1:1:1:1**		**3:3:2:2/4:2:2:2/6:1:1:1/2:2:2:2/2.5:2.5:2.5:2.5**					

		×	$Cu_{10.57}Ni_{5.63}Co_{3.14}Zn_{0.67}$	×					
	Cu-Ni-Co-Zn-Mn	**6:1:1:1:1**		**4:2:2:1:1**		**3:3:2:1:1**		**2:2:2:2:2**	
		$Cu_{12.89}Ni_{2.93}Co_{2.88}Zn_{1.12}Mn_{0.18}$	$Cu_{11.55}Ni_{3.91}Co_{3.39}Zn_{0.74}Mn_{0.44}$	$Cu_{9.98}Ni_{5.16}Co_{4.35}Zn_{0.41}Mn_{0.10}$	$Cu_{10.6}Ni_{5.12}Co_{3.98}Zn_{0.26}Mn_{0.48}$	$Cu_{9.06}Ni_{4.93}Co_{5.63}Zn_{0.23}Mn_{0.15}$	$Cu_{9.68}Ni_{4.45}Co_{5.19}Zn_{0.20}Mn_{0.48}$	$Cu_{9.37}Ni_{6.01}Co_{4.10}Zn_{0.39}Mn_{0.13}$	×
Amine		**A1**	**A2**	**A1**	**A2**	**A1**	**A2**	**A1**	**A2**

[a] A1: *iso*-propylamine, A2: trimethylamine [b] ×: Failed to obtain single crystals [c] -: Not yet tried

Table S3: ICP results of **M20-24** obtained in different batches.

M20-24	
11.55:3.91:3.39:0.74:0.44	1_{st}: 11.62:3.79:3.30:0.86:0.43
	2_{nd}: 11.69:3.82:3.37:0.63:0.49
	3_{rd}: 11.34:4.11:3.43:0.73:0.39

Table S4. ICP results of crystal samples from using equivalent amounts of starting metal salts.

Code	Ratio of starting metal acetates[a]	Ratio of metal number in $\{M_{20}\}$ clusters	Conclusion from the ICP results
M20-9	**1:1**	$Cu_{10.77}Co_{9.23}$	Cu > Co
M20-17	**3**:2:**3**	$Cu_{10.19}Ni_{4.91}Co_{4.90}$	Cu > Co
M20-19	**1:1:1:1**	$Cu_{10.57}Ni_{5.63}Co_{3.13}Zn_{0.67}$	Zn < Cu > Ni > Co
M20-20	6:**1:1**:1:1	$Cu_{12.87}Ni_{2.93}Co_{2.88}Zn_{1.12}Mn_{0.18}$	Ni > Co > Mn
M20-21	4:**2:2**:1:1	$Cu_{9.98}Ni_{5.16}Co_{4.35}Zn_{0.41}Mn_{0.10}$	Ni > Co
M20-22	**3**:2:**3**:1:1	$Cu_{9.06}Ni_{4.93}Co_{5.63}Zn_{0.23}Mn_{0.15}$	Cu > Co
M20-23	**2:2:2:2:2**	$Cu_{9.37}Ni_{6.01}Co_{4.10}Zn_{0.39}Mn_{0.13}$	Mn < Co < Ni < Cu > Zn
M20-24	6:**1:1**:1:1	$Cu_{11.55}Ni_{3.91}Co_{3.39}Zn_{0.74}Mn_{0.44}$	Ni > Co > Mn
M20-25	4:**2:2**:1:1	$Cu_{10.16}Ni_{5.12}Co_{3.98}Zn_{0.26}Mn_{0.48}$	Ni > Co
M20-26	**3**:2:**3**:1:1	$Cu_{9.68}Ni_{4.45}Co_{5.19}Zn_{0.20}Mn_{0.48}$	Cu > Co

[a]The bold number in “Ratio of starting metal acetates” column means the equal ratio of starting salts. They are help to compare the cooperation ability of metal elements within the clusters.

225

226

227

228

229 X-Ray Crystallographic Analysis

230 Single-crystal X-ray analyses were performed on a Siemens SMART platform diffractometer
231 outfitted with an Apex II area detector and monochromatized $Mo_{K\alpha}$ radiation (λ = 0.71073 Å).
232 Structures were solved by direct methods and refined using the *SHELXTL* software package.[1]

233

234 **Table S5.** Crystallographic data and structure refinement for **M20-7**, **M20-17** and **M20-24**

	M20-7	**M20-17**	**M20-24**
empirical formula	$C_{31}H_{94}Cu_{10.20}Ni_{9.80}O_{69}$	$C_{31}H_{94}Co_{4.90}Cu_{10.2}Ni_{4.90}O_{69}$	$C_{31}H_{93}Cu_{11.31}Co_{3.45}Mn_{0.39}Ni_{4.15}Zn_{0.69}O_{69}$
fw (g)	2794.53	2795.61	2802.47
T (K)	173 K	173 K	173 K
cryst syst	cubic	cubic	cubic
space group	Im-3m	Im-3m	Im-3m
*a (*Å)	17.1976(4)	17.2801	17.2463(2)
b (Å)	17.1976(4)	17.2801	17.2463(2)
c (Å)	17.1976(4)	17.2801	17.2463(2)
A(deg)	90	90	90
β(deg)	90	90	90
γ (deg)	90	90	90
V (Å^3)	5086.3(2)	5159.87(10)	5129.65(10)

Z	2	2	2
Dcalcd (g cm^{-3})	1.825	1.799	1.814
μ(mm^{-1})	3.943	3.781	3.871
F(000)	2804	2795	2798
R (>2ó(*I*))	R_1 = 0.1166	R_1 = 0.0738	R_1 = 0.0845
	wR_2 = 0.2788	wR_2 = 0.2632	wR_2 = 0.2752
GOF	*1.403*	*1.105*	*1.079*

252

253

254 **Table S6.** MOR performance comparison with pervious works

Catalysts	Electrolyte Concentration (M)	Scan rate ($mV\ s^{-1}$)	Activity at 0.75 V vs. Ag/AgCl(3.5 M KCl) ($mA \cdot cm^{-2}$)	Other potential and corresponding current density	Ref.
2Cu@CoOx-CLs	CH_3OH: 0.5 KOH: 1	50	108.25	-	[2]
$Ni_{0.75}Cu_{0.25}$	CH_3OH: 0.5 NaOH: 1	50	116.75	-	[3]
Cu/N-C monolith	CH_3OH: 0.5 KOH: 1	-	-	59.61$mA \cdot cm^{-2}$ at 0.569V	[4]
Cu–Ni NWs	CH_3OH: 0.5 NaOH: 1	50	133.19	-	[5]
CuO/$Co(OH)_2$ Nanosheets	CH_3OH: 3 KOH: 1	50	-	142$mA \cdot cm^{-2}$ at 0.60V	[6]
Cu/NiCu NWs	CH_3OH: 1 KOH: 1	50	-	33.33$mA \cdot cm^{-2}$ at 0.51V	[7]
CuO-NS	CH_3OH: 1 NaOH: 0.5	50	1.48	-	[8]
CuO/$Cu(OH)_2$ Nanoneedles	CH_3OH: 0.5 KOH: 1	5	-	120.91$mA \cdot cm^{-2}$ at 0.66V	[9]
$Cu(OH)_2$–CuO Nanoneedle Array	CH_3OH: 0.5 KOH: 1	10	-	60.3$mA \cdot cm^{-2}$ at 0.58V	[10]
Ni-Co	CH_3OH: 0.5 KOH: 1	50	-	36.42$mA \cdot cm^{-2}$ at 0.6V	[11]

$NiCo_2O_4$/rGO	CH_3OH: 0.5 NaOH: 1	50	-	5.23mA·cm^{-2} at 0.5V	12
Ni@3DHPG	CH_3OH: 0.5 KOH: 1	50	-	144.92mA·cm^{-2} at 0.7V	13
Ni-NPs/ZrO_2–PCs	CH_3OH: 0.5 KOH: 1	50		117.57mA·cm^{-2} at 0.6V	14
5CeO_2–NiO	CH_3OH: 1 KOH: 1	50	110.91		15
ZnCo2O4/Ni foam	CH_3OH: 0.5 KOH: 1	50	-	114.72mA·cm^{-2} at 0.6V	16
This work	CH_3OH: 0.5 KOH: 1	50	179.65	123.83mA·cm^{-2} at 0.6V	

[a]The potential of SCE or other reference electrodes are all transferred to Ag/AgCl according to SHE for easy comparison. The current density of methanol oxidation activity is obtained by using total current subtracting baseline current of OER in all data.

NoteS1: The Description of IR spectroscopy and TGA results

For the M20-20, the peaks at 681.9 cm^{-1}, 530 cm^{-1} and 1020 cm^{-1} attributed to the vibration of M-O (M: Cu, Ni, Co, Zn, Mn). Two peaks at 1413.8 cm^{-1} and 1570.1 cm^{-1} are the characteristic peak of methanol and acetonitrile. There is a board peak at around 3400-3500 cm^{-1} which origins from the vibration of coordination water molecules and oxhydryl group inside the crystal. From the spectra, it can be clearly seen the similarity of M20-7/M20-9, M20-17/M20-20. Figure S5 is the thermal gravimetric analysis (TGA) results of three samples. For M20-20, showed in Figure S5c the existence of the coordination water molecules was proved by the rapid weight decreasing between 20-180℃., which is caused by the loss of coordination water molecules and acetate ions. The second weight loss step at 180-350℃ assigned to the decomposition of ligands and oxhydryl group. After 350℃, a slow weight loss shows the formation of metal or metal oxide. The M20-7 and M20-17 (Figure S5a and b) own a similar pattern to M20-20 again verifying the structure resemblance.

NoteS2: Confirm of the Current Origin of NCNT-M20-20 2:1

Double-step chronoamperometry method was chosen to confirm the current density origin. As shown in Figure S11c, by switching potential from +0.6 V to +0.1 V (vs. Ag/AgCl) in a solution of 1 M KOH, no distinct reaction occurred (black line) for NCNT-M20-20 2:1 except limited OER process. However, when methanol was added (red line) the current density had a significant rise at +0.6 V but disappeared when switched back to +0.1 V, which strongly proves the origin of the current is from methanol oxidation compared to the blank one. The NCNT-Cu_{20} also showed a weak current response to methanol (blue line).

NoteS3: Surface Coverage Species Calculation

The surface coverage of Ni^{2+}-Ni^{3+} can be evaluated based on the equation below[17]:

$$I\mathrm{p} = \left(\frac{n^2F^2}{4RT}\right)vA\Gamma^{*}$$

Where Ip, F, R, T, v, A, Γ* represent peak current, the number of transferred electron(n=1), the general gas constant (8.314 $J\cdot K^{-1}\cdot mol^{-1}$), the temperature (298K), the scan rate (50 mV/s), the geometric area of glass carbon electrode (0.0706 cm^2), and surface coverage of the redox species. The linear relation of current density and scan rate is demonstrated in the inset graph of Figure.S12 (c), (d) and (e). The calculated Ni^{3+} Γ* of NCNT-M20-20 1:1, NCNT-M20-20 2:1, NCNT-M20-20 3:1 are 2.877×10^{-7} $mol\cdot cm^{-2}$, 1.197×10^{-6} $mol\cdot cm^{-2}$, 1.377×10^{-7} $mol\cdot cm^{-2}$ respectively.

NoteS4: CV Test to Understand Electrochemical Species Behavior

As shown in Figure S12b for NCNT-M20-20 2:1 in the forward scan, the wide peak at about +0.35 V (vs. Ag/AgCl) can be the signal of Ni^{2+}-Ni^{3+} redox couple. After +0.5 V there is a rapid current rise because of the severe water oxidation. In the backward scan, the wide peak at +0.25 V should be attributed to the reduction process of Ni^{3+}. And there is a board reduction peak around +0.5 V resulting from Cu^{2+}--Cu^{3+} redox couple which drifts to the negative side compared with NCNT-Cu_{20}. The shift may be attributed to the remaining elements consisted of M20-20 changed the chemical environment of Cu element. For NCNT-Cu_{20}, as the single metal component material, there is only a board reduction peak around +0.55 V owing to the Cu^{2+}--Cu^{3+} redox couple.[18]

For the CV tests of NCNT-M20-20 2:1 and 1:1 and 3:1 at different scan rates (Figure S12c, d, e), the anodic peaks shift to the positive side and cathodic peaks move to the negative with increasing of the scan rate. Figure S14d and e show a similar pattern with Figure S14c. NCNT-Cu_{20} (Figure S12a) won't be discussed because no Ni element in the compound but still has a similar trend. This phenomenon can be assigned to slow reaction kinetics resulted from the longer conversion time of Ni^{3+}-Ni^{2+} redox. The inset graphs in Figure S12c, d, e are the plot of

the anodic current density as the function of scan rate revealing a good linear correlation, which demonstrates that the conversion of Ni^{2+}-Ni^{3+} in KOH is a surface-controlled process.

The methanol electrooxidation is a kinetically controlled gas evolution reaction that the kinetic current won't change with scan rate,[18] as shown in Figure S12f with increasing scan rate the oxidation current changed inappreciably. Oppositely in the inset graph, a reduction peak is observed that the current density changed distinctly along with the scan rate. The reduction peak is attributed to Ni^{2+}-Ni^{3+} redox, in line with the former conclusion that conversion of Ni^{2+}-Ni^{3+} is a surface-controlled process drawn from Figure S14c.

NoteS5: The Electrochemical Active Surface Area and High Methanol Concentration Tolerance

Electrochemical active surface area (ECSA) is another index to evaluate electrochemical performance. The ECSA was obtained through a non-faraday section CV measurement at scan rate from 10 to 100 mV s^{-1} between 0 to +0.1 V (vs Ag/AgCl) as demonstrated in Figure S14. The results were calculated according to the equation: ECSA = C_{dl}/Cs, where C_{dl} represents electric double layer capacitance, Cs is the specific capacitance of 1 cm^2 atomically smooth standard electrode (here Cs = 0.04 mF·cm^{-2}).[19] C_{dl} of all tested subjects are shown in Figure.S11(b). The ECSA of NCNT-M20-20 2:1 is 427.00 cm^2 which is the highest among others where NCNT-M20-20 1:1, NCNT-M20-20 3:1, NCNT-Cu_{20} are 188.00, 142.50, 264.00 cm^2 respectively. Besides, NCNT-Cu_{20} has a similar ECSA with NCNT-M20-20 2:1 but with a poor performance, which hints the multicomponent played a vital rule in the MOR.

Catalyst performance in high concentration of methanol is an essential parameter for DMFC and practical pollutant removal. The property at high concentration was tested with the methanol concentration from 0.5-4 M (Figure S13a, b). The current density of NCNT-Cu_{20} keeps rising from 0.5 to 3 M, but a sudden fall at 4 M, shows in inset graph. For NCNT-M20-20 2:1 the current density keeps rising till as high as 4 M methanol (inset graph), indicating superior tolerance of methanol. The high concentration tolerance could be attributed to the quick conversion from intermediate that poisoning the electrode to the final CO_2 and H_2O. Assembled elements with hybridized d orbitals strengthen electronic interaction among the different components so that accelerate the redox process. These factors lead to enhanced catalytic performance of the catalyst.

{M_{20}} Library Synthesis Details

Synthesis of M20-7

A measured amount of trimethylamine (800 μL) was added to the mixture of $Cu(OAc)_2 \cdot H_2O$

(0.1996 g, 1 mmol) $Ni(OAc)_2{\cdot}4H_2O$ (0.3732 g, 1.5 mmol) in CH_3CN (20 mL). The solution was stirred at room temperature for 24 h and then filtered. The filtrate was evaporated to give green solid in two days. Recrystallization in CH_3OH produces single crystals suitable for X-ray analysis.Yield: ca. 60 % (based on Cu). Elemental analysis found (%) for $Cu_{10.38}Ni_{9.62}$: Cu 18.5071, Ni 15.8391.

Synthesis of M20-9

A measured amount of triethylamine (800 μL) and H_2O (100 μL) were added tothe mixture of $Cu(OAc)_2{\cdot}H_2O$ (0.1996 g, 1 mmol), $Co(OAc)_2{\cdot}4H_2O$ (0.2491 g, 1mmol) in CH_3CN (20 mL). The solution was stirred at room temperature for 24h to form a gel, added CH_3OH (10 mL). The filtrate was evaporated to givewell-formed dark gray crystals in one weeks. The crystals were collected by filtration, washed with MeOH and air-dried. Yield: ca. 60 % (based on Cu). Elemental analysis found (%) for $Cu_{10.77}Co_{9.23}$: Cu 23.2214, Co 18.4736.

Synthesis of M20-10

A measured amount of triethylamine (800 μL) and H_2O (100 μL) were added to the mixture of $Cu(OAc)_2{\cdot}H_2O$ (0.1996 g, 1 mmol), $Co(OAc)_2{\cdot}4H_2O$ (0.3737 g, 1.5 mmol) in CH_3CN (20 mL). The solution was stirred at room temperature for 24 hours to form a gel, added CH_3OH (10mL). The filtrate was evaporated to give well-formed dark gray crystals in one weeks. The crystals were collected by filtration, washed with MeOH and air-dried. Yield: ca. 60 % (based on Cu). Elemental analysis found (%) for $Cu_{9.80}Co_{10.20}$: Cu 22.2018, Co 21.4283.

Synthesis of M20-17

A measured amount of *iso*-$C_3H_7NH_2$ (400 μL) and H_2O (400 μL) were added tothe mixture of $Cu(OAc)_2{\cdot}H_2O$ (0.5988 g, 3 mmol), $Ni(OAc)_2{\cdot}4H_2O$ (0.4976 g, 2 mmol), $Co(OAc)_2{\cdot}4H_2O$ (0.7473 g, 3 mmol) in CH_3CN (20 mL). The solution was stirred at room temperature for 24 h, added CH_3OH (20 mL). The filtrate was evaporated to give dark powder crystal in a week. Recrystallizationin CH_3OH produces single crystals suitable for X-ray analysis. After several days, the gray crystals were obtained by filtration, washed with CH_3CH_2OH and air-dried. Yield: ca. 60 % (based on Cu). Elemental analysis found (%) for$Cu_{10.19}Ni_{4.91}Co_{4.90}$: Cu 20.8225, Ni 9.2662, Co 9.29562.

Synthesis of M20-19

A mixture of $Cu(OAc)_2 \cdot H_2O$ (0.1996 g, 1 mmol), $Co(OAc)_2 \cdot 4H_2O$ (0.2491 g, 1mmol), $Ni(OAc)_2 \cdot 4H_2O$ (0.2485 g, 1 mmol), $Zn(OAc)_2 \cdot H_2O$ (0.2195 g, 1 mmol) was dissolved in CH_3CN (20 mL). Gradually added in triethylamine (2 ml) and H_2O (400 μL) while stirring. The mixture was stirred at room temperature for 24 h. The filtrate was evaporated to give well-formed gel in a week. Recrystallization in CH_3OH twice produces single crystals suitable for X-ray analysis. After several days, the gray crystals were obtained by filtration, washed with CH_3CH_2OH and air-dried. Yield: ca. 60 % (based on Cu). Elemental analysis found (%) for $Cu_{10.57}Ni_{5.63}Co_{3.14}Zn_{0.67}$: Cu 25.0532, Ni 12.3184, Co 6.8893, Zn 1.6524.

Synthesis of M20-20

A mixture of $Cu(OAc)_2 \cdot H_2O$ (1.1976 g, 6 mmol), $Co(OAc)_2 \cdot 4H_2O$ (0.2491 g, 1mmol), $Ni(OAc)_2 \cdot 4H_2O$ (0.2485 g, 1 mmol), $Zn(OAc)_2 \cdot H_2O$ (0.2195 g, 1 mmol),$Mn(OAc)_2 \cdot 4H_2O$ (0.2451 g, 1 mmol) was dissolved in CH_3CN (20 mL). Gradually added in *iso*-$C_3H_7NH_2$ (2 ml) and H_2O (400 μL) while stirring. The mixture was stirred at room temperature for 24 h. The filtrate was evaporated to give well-formed gel in a week. Recrystallization in CH_3OH twice produces single crystals suitable for X-ray analysis. After several days, the gray crystals were obtained by filtration, washed with CH_3CH_2OH and air-dried. Yield: ca. 60 % (based on Cu). Elemental analysis found (%) for $Cu_{12.89}Ni_{2.93}Co_{2.88}Zn_{1.12}Mn_{0.18}$: Cu 27.3165, Ni 5.7244, Co 5.6515, Zn 2.4446, Mn 0.3297.

Synthesis of M20-21

A mixture of $Cu(OAc)_2 \cdot H_2O$ (0.7984 g, 4 mmol), $Co(OAc)_2 \cdot 4H_2O$ (0.4982 g, 2mmol, $Ni(OAc)_2 \cdot 4H_2O$ (0.4976 g, 2 mmol), $Zn(OAc)_2 \cdot H_2O$ (0.2195 g, 1 mmol), $Mn(OAc)_2 \cdot 4H_2O$ (0.2451 g, 1 mmol) was dissolved in CH_3CN (20 mL). Gradually added in iso-$C_3H_7NH_2$ (2 ml) and H_2O (400 μL) while stirring. The mixture was stirred at room temperature for 24 h. The filtrate was evaporated to give well-formed gel in a week. Recrystallization in CH_3OH twice produces single crystals suitable for X-ray analysis. After several days, the gray crystals were obtained by filtration, washed with CH_3CH_2OH and air-dried. Yield: ca.60 % (based on Cu). Elemental

analysis found (%) for $Cu_{9.98}Ni_{5.16}Co_{4.35}Zn_{0.41}Mn_{0.10}$: Cu 21.4387, Ni 10.2348, Co 8.6753, Zn 0.9112, Mn 0.1847.

Synthesis of M20-22

A mixture of $Cu(OAc)_2 \cdot H_2O$ (0.5988 g, 3 mmol), $Co(OAc)_2 \cdot 4H_2O$ (0.7473 g, 3mmol), $Ni(OAc)_2 \cdot 4H_2O$ (0.4976 g, 2 mmol), $Zn(OAc)_2 \cdot H_2O$ (0.2195 g, 1 mmol), $Mn(OAc)_2 \cdot 4H_2O$ (0.2451 g, 1 mmol) was dissolved in CH_3CN (20 mL). Gradually added in iso-$C_3H_7NH_2$ (2 ml) and H_2O (400 μL) while stirring. The mixture was stirred at room temperature for 24 h. The filtrate was evaporated to give well-formed gel in a week. Recrystallization in CH_3OH twice produces single crystals suitable for X-ray analysis. After several days, the gray crystals were obtained by filtration, washed with CH_3CH_2OH and air-dried. Yield: ca.60 % (based on Cu). Elemental analysis found (%) for $Cu_{9.06}Ni_{4.93}Co_{5.63}Zn_{0.23}Mn0_{.15}$: Cu 20.2308, Ni 10.1665, Co 11.6568, Zn 0.5211, Mn 0.2983.

Synthesis of M20-23

A mixture of $Cu(OAc)_2 \cdot H_2O$ (0.3992 g, 2 mmol), $Co(OAc)_2 \cdot 4H_2O$ (0.4982 g, 2mmol), $Ni(OAc)_2 \cdot 4H_2O$ (0.4976 g, 2 mmol), $Zn(OAc)_2 \cdot H_2O$ (0.4390 g, 2 mmol), $Mn(OAc)_2 \cdot 4H_2O$ (0.2451 g, 2 mmol) was dissolved in CH_3CN (20 mL). Gradually added in *iso*-$C_3H_7NH_2$ (2 ml) and H_2O (400 μL) while stirring. The mixture was stirred at room temperature for 24 h. The filtrate was evaporated to give well-formed gel in a week. Recrystallization in CH_3OH twice produces single crystals suitable for X-ray analysis. After several days, the gray crystals were obtained by filtration, washed with CH_3CH_2OH and air-dried. Yield: ca.60 % (based on Cu). Elemental analysis found (%) for $Cu_{9.37}Ni_{6.01}Co_{4.10}Zn_{0.39}Mn_{0.12}$: Cu 20.0480, Ni 11.8846, Co 8.1353, Zn 0.8673, Mn 0.2301.

Synthesis of M20-24

A mixture of $Cu(OAc)_2 \cdot H_2O$ (1.1976 g, 6 mmol), $Co(OAc)_2 \cdot 4H_2O$ (0.2491 g, 1 mmol), $Ni(OAc)_2 \cdot 4H_2O$ (0.4976 g, 1 mmol), $Zn(OAc)_2 \cdot H_2O$ (0.2195 g, 1 mmol), $Mn(OAc)_2 \cdot 4H_2O$ (0.2451 g, 1 mmol) was dissolved in CH_3CN (20 mL). Gradually added in triethylamine (2 ml) and H_2O (400 μL) while stirring. The mixture was stirred at room temperature for 24 h. The filtrate was evaporated to give well-formed gel in a week. Recrystallization in CH_3OH twice produces single

crystals suitable for X-ray analysis. After several days, the gray crystals were obtained by filtration, washed with CH_3CH_2OH and air-dried. Yield: ca.60 % (based on Cu). Elemental analysis found (%) for $Cu_{11.55}Ni_{3.99}Co_{3.39}Zn_{0.74}Mn_{0.44}$: (a) Cu 26.2967, Ni 8.0627, Co 7.1332, Zn 1.4970, Mn 0.9674; (b) Cu 27.6739, Ni 8.3407, Co 7.2818, Zn 2.1253, Mn 0.8846; (c) Cu 22.9484, Ni 7.6913, Co 6.4329, Zn 1.5176, Mn 0.6787.

Synthesis of M20-25

A mixture of $Cu(OAc)_2 \cdot H_2O$ (0.7984 g, 4 mmol), $Co(OAc)_2 \cdot 4H_2O$ (0.4982 g, 2 mmol), $Ni(OAc)_2 \cdot 4H_2O$ (0.4976 g, 2 mmol), $Zn(OAc)_2 \cdot H_2O$ (0.2195 g, 1 mmol), $Mn(OAc)_2 \cdot 4H_2O$ (0.2451 g, 1 mmol) was dissolved in CH_3CN (20 mL). Gradually added in triethylamine (2 ml) and H_2O (400 μL) while stirring. The mixture was stirred at room temperature for 24 h. The filtrate was evaporated to give well-formed gel in a week. Recrystallization in CH_3OH twice produces single crystals suitable for X-ray analysis. After several days, the gray crystals were obtained by filtration, washed with CH_3CH_2OH and air-dried. Yield: ca. 60 % (based on Cu). Elemental analysis found (%) for $Cu_{10.16}Ni_{5.12}Co_{3.98}Zn_{0.26}Mn_{0.48}$: Cu 21.4963, Ni 10.0089, Co 7.8094, Zn 0.5701,Mn 0.8711.

Synthesis of M20-26

A mixture of $Cu(OAc)_2 \cdot H_2O$ (0.5988 g, 3 mmol), $Co(OAc)_2 \cdot 4H_2O$ (0.4982 g, 2 mmol), $Ni(OAc)_2 \cdot 4H_2O$ (0.7464 g, 3 mmol), $Zn(OAc)_2 \cdot H_2O$ (0.2195 g, 1 mmol),$Mn(OAc)_2 \cdot 4H_2O$ (0.2451 g, 1 mmol) was dissolved in CH_3CN (20 mL). Gradually added in triethylamine (2 ml) and H_2O (400 μL) while stirring. The mixture was stirred at room temperature for 24 h. The filtrate was evaporated to give well-formed gel in a week. Recrystallization in CH_3OH twice produces single crystals suitable for X-ray analysis. After several days, the gray crystals were obtained by filtration, washed with CH_3CH_2OH and air-dried. Yield: ca. 60 % (based on Cu). Elemental analysis found (%) for $Cu_{9.68}Ni_{4.45}Co_{5.19}Zn_{0.20}Mn_{0.48}$: Cu 20.4417, Ni 8.6738, Co 10.1624, Zn 0.4435, Mn 0.8723.

References

1. G. Sheldrick, *University of Göttingen, Göttingen, Germany (2008)*, 1997.

2. Y. Sun, Y. Zhou, C. Zhu, W. Tu, H. Wang, H. Huang, Y. Liu, M. Shao, J. Zhong, S.-T. Lee and Z. Kang, *Appl. Catal., B*, 2019, **244**, 795-801.

3. X. Cui, P. Xiao, J. Wang, M. Zhou, W. Guo, Y. Yang, Y. He, Z. Wang, Y. Yang and Y. Zhang, *Angew. Chem. Int. Ed.*, 2017, **129**, 4559-4564.

4. F. Chen, N. Wu, M. Zhai, X. Zhang, R. Guo, T. Hu and M. Ma, *J. Energy Chem.*, 2021, **58**, 247-255.

5. W. Tong, Q. Shao, P. Wang and X. Huang, *Chem. Eur. J.*, 2019, **25**, 7218-7224.

6. L. Chen, Z. Hua, J. Shi and M. He, *ACS Appl. Mater. Interfaces*, 2018, **10**, 39002-39008.

7. D. Wu, W. Zhang and D. Cheng, *ACS Appl. Mater. Interfaces*, 2017, **9**, 19843-19851.

8. A. P. M. Udayan and S. N. Sawant, *J. Phys. Chem. Solids*, 2021, **150**, 109883.

9. S. Anantharaj, H. Sugime, S. Yamaoka and S. Noda, *ACS Appl. Energy Mater.*, 2021, **4**, 899-912.

10. S. Anantharaj, H. Sugime and S. Noda, *ACS Appl. Mater. Interfaces*, 2020, **12**, 27327-27338.

11. G. S. Theres, G. Velayutham, C. Suresh, P. S. Krishnan and K. Shanthi, *J. Appl. Electrochem.*, 2020, **50**, 639-653.

12. M. B. Askari and P. Salarizadeh, *J. Mol. Liq.*, 2019, **291**, 111306.

13. N. Ullah, M. Xie, C. J. Oluigbo, Y. Xu, J. Xie, H. U. Rasheed and M. Zhang, *J. Electroanal. Chem.*, 2019, **838**, 7-15.

14. S. Sheikhi and F. Jalali, *Int. J. Hydrogen Energy*, 2021, **46**, 10723-10738.

15. W. Li, Z. Song, X. Deng, X.-Z. Fu and J.-L. Luo, *Electrochim. Acta*, 2020, **337**, 135684.

16. R. Shi, Y. Zhang and Z. Wang, *J. Alloys Compd.*, 2019, **810**, 151879.

17. A. A. Dubale, Y. Zheng, H. Wang, R. Hübner, Y. Li, J. Yang, J. Zhang, N. K. Sethi, L. He, Z. Zheng and W. Liu, *Angew. Chem., Int. Ed.*, 2020, **59**, 13891-13899.

18. S. Anantharaj, H. Sugime and S. Noda, *ACS Appl. Mater. Interfaces*, 2020, **12**, 27327-27338.

19. M. Wang, C. Wang, L. Zhu, F. Rong, L. He, Y. Lou and Z. Zhang, *Appl. Catal., A*, 2021, **619**, 118159.

502